[18F]F-DPA for the detection of activated microglia in a mouse model of Alzheimer's disease

Thomas Keller, Francisco R López-Picón, Anna Krzyczmonik, Sarita Forsback, Anna K Kirjavainen, Jatta S Takkinen, Obada Alzghool, Johan Rajander, Simo Teperi, Fanny Cacheux, et al.

Nuclear Medicine and Biology 67 (2018) 1–9

Contents lists available at ScienceDirect

Nuclear Medicine and Biology

journal homepage: www.elsevier.com/locate/nucmedbio

[^{18}F]F-DPA for the detection of activated microglia in a mouse model of Alzheimer's disease☆

Thomas Keller [a,*], Francisco R. López-Picón [b,c], Anna Krzyczmonik [a], Sarita Forsback [a,d], Anna K. Kirjavainen [a], Jatta S. Takkinen [b,c], Obada Alzghool [b,c], Johan Rajander [e], Simo Teperi [f], Fanny Cacheux [g], Annelaure Damont [g], Frédéric Dollé [g], Juha O. Rinne [h], Olof Solin [a,d,e], Merja Haaparanta-Solin [b,c]

[a] Radiopharmaceutical Chemistry Laboratory, Turku PET Centre, University of Turku, Finland
[b] PET Preclinical Imaging Laboratory, Turku PET Centre, University of Turku, Finland
[c] MediCity Research Laboratory, University of Turku, Finland
[d] Department of Chemistry, University of Turku, Finland
[e] Accelerator Laboratory, Turku PET Centre, Åbo Akademi University, Finland
[f] Department of Biostatistics, University of Turku, Finland
[g] CEA, I2BM, Service Hospitalier Frédéric Joliot, Orsay, France
[h] Turku PET Centre, Division of Clinical Neurosciences, Turku University Hospital, Turku, Finland

ARTICLE INFO

Article history:
Received 29 June 2018
Received in revised form 3 September 2018
Accepted 23 September 2018

Keywords:
TSPO
APP/PS1-21
Neuroinflammation
PET
Fluorine-18
F-DPA

ABSTRACT

Introduction: Neuroinflammation is associated with several neurological disorders, including Alzheimer's disease (AD). The translocator protein 18 kDa (TSPO), due to its overexpression during microglial activation and relatively low levels in the brain under normal neurophysiological conditions, is commonly used as an *in vivo* biomarker for neuroinflammation. Reported here is the preclinical evaluation of [^{18}F]F-DPA, a promising new TSPO-specific radioligand, as a tool for the detection of activated microglia at different ages in the APP/PS1-21 mouse model of AD and a blocking study to determine the specificity of the tracer.
Methods: [^{18}F]F-DPA was synthesised by the previously reported electrophilic ^{18}F-fluorination methodology. *In vivo* PET and *ex vivo* brain autoradiography were used to observe the tracer distribution in the brains of APP/PS1-21 and wildtype mice at different ages (4.5–24 months). The biodistribution and degree of metabolism of [^{18}F]F-DPA were analysed and the specificity of [^{18}F]F-DPA for its target was determined by pre-treatment with PK11195.
Results: The *in vivo* PET imaging and *ex vivo* brain autoradiography data showed that [^{18}F]F-DPA uptake in the brains of the transgenic animals increased with age, however, there was a drop in the tracer uptake at 19 mo. Despite the slight increase in [^{18}F]F-DPA uptake with age in healthy animal brains, significant differences between wildtype and transgenic animals were seen *in vivo* at 9 months and *ex vivo* already at 4.5 months. The specificity study demonstrated that PK11195 can be used to significantly block [^{18}F]F-DPA uptake in all the brain regions studied.
Conclusions: In vivo time activity curves plateaued at approximately 20–40 min suggesting that this is the optimal imaging time. Significant differences *in vivo* are seen at 9 and 12 mo. Due to the higher resolution, *ex vivo* autoradiography with [^{18}F]F-DPA can be used to visualise activated microglia at an early stage of AD pathology.

1. Introduction

Neuroinflammation has, for a long time, been associated with a wide range of neurological diseases and conditions, amongst them stroke, multiple sclerosis and Alzheimer's disease (AD). When neuroinflammation occurs, microglia are activated in an attempt to protect the nervous tissue from the damage. The translocator protein 18 kDa (TSPO), formerly known as the peripheral benzodiazepine receptor [1], is located primarily on the outer mitochondrial membrane [2]. Due to its overexpression during microglial activation and relatively low levels in the brain under normal neurophysiological conditions [3,4], the TSPO has been adopted as a biomarker for neuroinflammation.

The past two decades have seen the development and use of numerous TSPO-specific positron emission tomography (PET) tracers for the imaging of various diseases, such as; herpes encephalitis [5,6], glioma [7], rheumatoid arthritis [8], multiple sclerosis [9], and AD [9,10], to

☆ This is a free access article and can be viewed on the journal's Web site (www.nucmedbio.com). Complimentary access to this article is available until the next issue publishes online.

* Corresponding author at: Turku PET Centre, University of Turku, Kiinamyllynkatu 4-8, FI-20520 Turku, Finland.
E-mail address: tomkel@utu.fi (T. Keller).

https://doi.org/10.1016/j.nucmedbio.2018.09.001

name a few. Despite the existence of several clinically used TSPO-specific radioligands, the development of novel tracers with higher signal-to-noise ratio is paramount for increasing the quality of PET images and data, particularly in diseases which exhibit a low signal. One of the latest additions to this library of tracers is the recently reported *N*,*N*-diethyl-2-(2-(4-([^{18}F]fluoro)phenyl)-5,7-dimethylpyrazolo[1,5-*a*]pyrimidin-3-yl)acetamide ([^{18}F]F-DPA), initially synthesised by an electrophilic method from a stannylated precursor using [^{18}F]Selectfluor *bis*(triflate) [11]. [^{18}F]F-DPA has already attracted much interest and has undergone evaluation by Wang et al. in an animal model of stroke and briefly (n = 2) in the APP/PS1 model of AD [12]. [^{18}F]F-DPA is an analogue of the well-known tracer [^{18}F]DPA-714 [13]. [^{18}F]DPA-714 has previously been employed in neuroinflammation PET studies [14] with the APP/PS1-21 mouse model of AD, as has the related tracer [^{18}F]PBR111 [15]. The mutations in this animal model result in the formation Aβ plaques at approximately 2 months (mo) of age, these plaques are accompanied by microglia activation and neuronal as well as cognitive degeneration [16,17].

In [^{18}F]DPA-714, the fluorine-18 label is found on the terminal position of an alkoxy chain, bonded to an aromatic moiety through the oxygen atom. However, this position has been shown to be unstable with respect to metabolism [9,18]. Nevertheless, this motif remains widely studied in the field of tracer discovery, resulting in the development of numerous related TSPO-specific PET ligands in recent years [19–22]. [^{18}F]F-DPA differs from [^{18}F]DPA-714 by the absence of the alkoxy linker between the label and the aromatic ring, *i.e.* the fluorine-18 atom is found directly on the aromatic ring, a position which confers a higher degree of stability with respect to radiometabolite formation by cleavage of the fluorine-18 atom.

We have previously reported the radiosynthesis and evaluation of [^{18}F]F-DPA in Sprague Dawley rats [11]. This comparison of [^{18}F]F-DPA and [^{18}F]DPA-714 demonstrated higher metabolic stability and favourable wash out kinetics for the new [^{18}F]F-DPA. Reported here is the further in-depth evaluation of [^{18}F]F-DPA in the APP/PS1-21 mouse model of AD. The tracer uptake was measured in both young and ageing AD mice by *in vivo* PET and *ex vivo* brain autoradiography. Additionally, this preclinical study includes an investigation of the metabolic profile of [^{18}F]F-DPA in mice and a blocking with PK11195 to demonstrate the specificity of [^{18}F]F-DPA uptake in the APP/PS1-21 mouse brain. This study is the first instance [^{18}F]F-DPA being used to image APP/PS1-21 AD model mice.

2. Materials and methods

2.1. Radiochemistry

N,*N*-diethyl-2-(2-(4-([^{18}F]fluoro)phenyl)-5,7-dimethylpyrazolo[1,5-*a*]pyrimidin-3-yl)acetamide ([^{18}F]F-DPA) was synthesised from 7.5 ± 2.32 GBq of [^{18}F]Selectfluor *bis*(triflate) (decay corrected to end of bombardment (EOB)) (Fig. 1) according to the same procedure as previously described [11]. The molar activity (A_m) of the product was 7.5 ± 2.3 GBq/μmol (decay corrected to EOB).

2.2. Animals

All of the animal experiments were approved by the Regional State Administrative Agency for Southern Finland (permission ESAVI/3899/04.10.07/2013 and ESAVI/4660/04.10.07/2016) and animal care complied with the guidelines of the International Council of Laboratory Animal Science (ICLAS). This study was performed with the APP/PS1-21 transgenic mouse model of AD (TG, n = 31, 15 males) and WT mice (WT, n = 19, 10 males) with ages ranging from 4.5 to 24 mo. APP/PS1-21 coexpresses KM670/671NL mutated amyloid precursor protein and a very aggressive presenilin 1 mutation (L166P) under the control of a neuron-specific Thy1 promoter. The Aβ42-driven cerebral amyloidosis starts at 6–8 wk, amyloid-associated pathologies including dystrophic synaptic boutons, hyperphosphorylated tau-positive neuritic structures and robust gliosis are also detected, with the number of neocortical microglia increasing threefold from 1 to 8 mo of age [16,17]. The original publication of the APP/PS1-21 animal model demonstrated that there was no difference between the amyloid load of depositing male and female mice at 2 mo [16]. Aβ immunoreactive plaques develop progressively in the neocortex and hippocampus, and are associated with dystrophic neurites and gliosis [17]. APP/PS1-21 mice were originally provided by KOESLER (Rottenburg, Germany) and were further bred in the Central Animal Laboratory of University of Turku with C57BL/6Cn mice.

All animals were group-housed under standard conditions (temperature 21 ± 3 °C, humidity 55 ± 15%, lights on from 6:00 a.m. until 6:00 p.m.) at the Central Animal Laboratory, University of Turku and had *ad libitum* access to soy-free chow (RM3 (E) soya-free, 801710, Special Diets Service) and tap water.

2.3. In vivo PET/CT imaging and analysis

PET imaging was performed with female and male TG (n = 22, 12 male, weight: 29.27 ± 5.95 g, aged 4.5–19 mo, n = 3–4 per age group) and WT mice (n = 19, 10 male, weight: 30.4 ± 7.24 g, aged 4.5–9 mo, n = 1–6 per age group), a detailed description of the groups has been presented in the supplementary material (Supplementary Table 1). The mice, anaesthetized with 2.5% isoflurane/oxygen gas, were injected intravenously (i.v.) with [^{18}F]F-DPA (6.91 ± 0.59 MBq, 0.05 ± 0.03 mg/kg) for scanning by Inveon multimodality PET/CT scanner (Siemens Medical Solutions, Knoxville, TN, USA). The mice were kept on a heating pad and under anaesthesia during the study.

The mice were first scanned for 10 min with computed tomography (CT) for attenuation correction and anatomical reference. Immediately after that a 60-min dynamic PET scan (51 frames: 30 × 10, 15 × 60, 4 × 300 and 2 × 600 s) was started and the tracer was injected intravenously *via* a tail vein.

For image analysis, dynamic PET images were first co-registered with corresponding CT images for a robust anatomical registration. The second, rigid registration was performed by aligning the PET/CT images with an averaged mouse MRI template [23] and, thus predefined standardised volumes of interest (VOIs) were placed in the neocortex (CTX), frontal cortex (FC), hippocampus (HIPP), cerebellar cortex (CB)

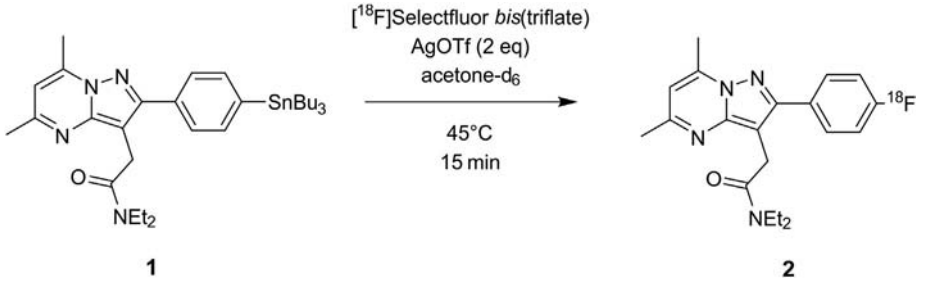

Fig. 1. Synthesis of ^{18}F-F-DPA (2) from stannylated precursor (1) using post-target produced [^{18}F]F_2 derived [^{18}F]Selectfluor *bis*(triflate).

and the whole brain (WB), with Inveon Research Workplace 4.2 (Siemens Medical Solutions) using the template as an anatomic reference. Averaged standardised uptake values (SUVs) were calculated for the 20–40 min washout phase.

2.4. Ex vivo brain autoradiography

Following the *in vivo* studies, while still under deep anaesthesia, the mice were sacrificed by cardiac puncture. Once removed, the whole brain was weighed and the radioactivity was measured using a gamma counter (Wizard^2 3 × 3″, PerkinElmer, Turku, Finland). The brain was then rapidly frozen in isopentane (Sigma-Aldrich) on dry ice. Preparation of brain slices for autoradiography and exposure was performed according to previously reported procedures [14,24].

After the exposure, the imaging plates were scanned using BAS-5000 reader (Fuji, Japan) with a resolution of 25 μm. The digitised images were analysed by AIDA Image Analyzer 4.5 software (Raytest, Isotopenmessgeräte, Straubenhardt, Germany). The regions-of-interest (ROIs) were drawn in the FC, HIPP, CB, lateral ventricle (LV) and hypothalamus (HYP). The ROIs were calculated as photostimulated intensity/area - background (PSL/mm^2) and presented as region-of-interest to hypothalamus (ROI/HYP) ratios. The HYP was used as the reference region due to reasons discussed later.

2.5. Blocking study

Three 15-mo-old TG mice were selected for a blocking study to determine the specificity of the [^{18}F]F-DPA binding. The animals were injected intraperitoneally with PK11195 (ABX GmbH, Radeberg, Germany; 1 mg total dose, in DMSO), 30 min prior to the administration of the tracer [25]. All mice were imaged by PET/CT for 60 min and, after that, sacrificed and the brains were sliced for autoradiography analyses.

2.6. Biodistribution

Following the sacrifice, the mice (5 min, n = 3; 15 min, n = 3; 30 min, n = 3, 60 min: n = 19, the 60 min animals had been used for *in vivo* PET imaging) previously injected i.v. with [^{18}F]F-DPA (6.84 ± 0.58 MBq, 0.05 ± 0.04 mg/kg) were dissected and the blood and organs were harvested for biodistribution studies. The tissues were weighed and the radioactivity was measured using the gamma counter (Wizard^2 3 × 3″). The activity is reported as the percentage of injected dose per gram of tissue (%ID/g tissue).

2.7. Radiometabolite TLC analysis

For radiometabolite analysis, blood and cortex samples were taken from the same mice used in the biodistribution studies. The preparation of samples and TLC analysis was carried out according to previously published methods [11].

2.8. Immunohistochemical staining

Microglial activation was assessed with the inflammation marker ionized calcium binding adaptor molecule 1 (Iba1) (Wako Ltd., Japan). The immunohistochemistry protocol was performed as described before [24].

2.9. Statistical methods

The results are reported as means ± standard deviation (n ≥ 3). The relationships between *in vivo* SUVs or *ex vivo* ROI/HYP ratios and the independent variables *group* (WT or TG) and *age* were studied with descriptive statistics and ANOVA model. Continuous variables were characterized using median and range of values. The main statistical analyses for *in vivo* SUVs or *ex vivo* ROI/HYP ratios were performed using the ANOVA model. Due to small sample size, separate models were used to evaluate some TG groups. *Group* and *age* were included in all models. p-Values were adjusted with Bonferroni correction to avoid Type 1 error. The p-values determined for the age matched comparison of WT and TG animals, both *in vivo* and *ex vivo*, have been provided in supplementary tables 2 and 3. Statistical significance level was set at 0.05 in all tests (two-tailed). The analyses were performed using SAS system, version 9.4 for Windows (SAS Institute Inc., Cary, NC, US).

The correlation between *in vivo* SUVs averaged over 20–40 min or *ex vivo* autoradiography ratios and age, as well as between *in vivo* SUVs averaged over 20–40 min and *ex vivo* autoradiography ratios was tested using the Pearson correlation coefficient and differences were considered statistically significant if the p value was <0.05.

3. Results

3.1. In vivo PET/CT imaging and analysis

The time-activity curves (TACs) for the TG mice (Fig. 2A) showed that, after the sharp initial peak, the level and speed at which the TAC reaches equilibrium differed depending on age. The younger age groups showed a fast washout and the tracer concentration reached equilibrium between 10 and 20 min after injection. In the older TG age groups, the initial uptake was followed by higher tracer-binding, hence the level at which the tracer concentration equilibrates increased with age until 12 mo. For these older age groups, the concentration equilibrium of the tracer was reached at 20–40 min after injection. There was little apparent difference between the curves of the 12 and 15 mo TG animals, however for the 19 mo TG animals, the binding of the tracer dropped relative to the 15 mo TG animals. For the WT mice, the level at which the equilibrium plateau was reached, increased between 4.5 and 12 mo, but there was no subsequent increase between 12 and 24 mo (Fig. 2B).

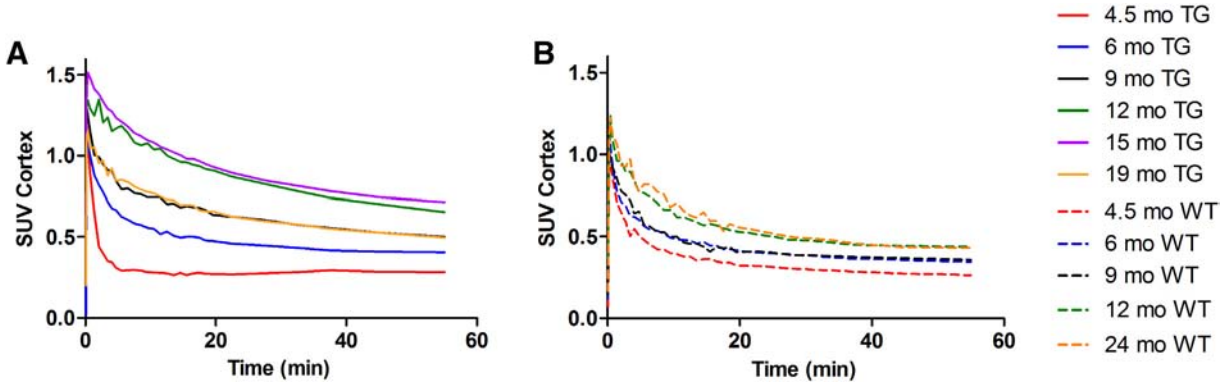

Fig. 2. Time-activity curves derived from the cortex VOIs for A) 4.5–19 mo TG n = 3–4 and B) 4.5–9 mo WT n = 1–6 per age group. Error bars have been omitted for the sake of clarity.

The SUVs, averaged during 20–40 min of the scan, for the FC, WB, CB and HIPP of TG mice, varied as a function of age. A significantly higher tracer uptake was observed in the FC, WB, and HIPP of 9 mo TG animals compared age-matched WT animals (Fig. 3A–D). At 12 mo TG animals showed significantly higher tracer uptake in all of the brain regions studied compared to the age matched WT animals. Example PET/CT images in the coronal plane, at the level of the HIPP are shown for 4.5 mo WT and 4.5, 9, 15 and 19 mo TG in Fig. 4.

Correlation between *in vivo* PET and age (Supplementary Fig. 1) showed that for the TG animals there is a strong positive correlation in all of the brain regions studied. In WT animals, a similar correlation was observed but at a lower level of statistical significance.

3.2. Ex vivo brain autoradiography and immunohistochemical staining

The *ex vivo* autoradiography images and in particular the immunohistochemical staining of the same brain slices (Fig. 4), demonstrated that the hypothalamus remains relatively clear of pathology which causes neuroinflammation, even in very old TG animals, and hence it could be employed as a reference region for the calculation of ROI/HYP ratios. These derived ROI/HYP ratios (Fig. 5) showed that there is already a highly significant difference between the uptake of [^{18}F]F-DPA in the FC in animals as young as 4.5 mo when compared to the age matched WT groups. There was an increase in the uptake in the FC and HIPP between 4.5 and 15 mo in the TG mice, subsequently there was a drop in the uptake at 19 mo. The ROI/HYP ratios of WT animals showed no significant variation with age. A comparison of the LV/HYP (Fig. 5C) ratios showed that there is no significant difference between age matched TG and WT.

The correlation between *ex vivo* autoradiography ratios and age (Supplementary Fig. 1) showed that for the TG animals there is a strong positive correlation. However WT animals demonstrated no correlation between autoradiography ratios and age.

Correlation carried out between *in vivo* PET and *ex vivo* autoradiography data for the FC and HIPP (Supplementary Fig. 2) showed that for the TG animals there is a clear positive correlation in both the FC ($r^2 = 0.6711$, $p < 0.0001$) and HIPP ($r^2 = 0.6612$ $p < 0.0001$). In contrast, in WT animals no correlation was seen in either FC ($r^2 = 0.006659$, $p = 0.7475$) or HIPP ($r^2 = 0.009929$ $p = 0.6940$).

3.3. Blocking study

When the *in vivo* and *ex vivo* images (Fig. 6) and derived cortical TACs (Fig. 7A) and ROI/HYP ratios (Fig. 7B) of 15 mo TG blocked mice were compared with those of the age-matched non-pretreated TG animals, a clear blocking and significant difference can be seen in all the brain regions studied. As would be expected, the TACs for the blocked TG animals strongly resemble those of the WT mice (Fig. 2A).

The blocking of TSPO with PK11195 resulted in significantly lower uptake ratios in all the brain regions studied (Fig. 7B). Notable is that

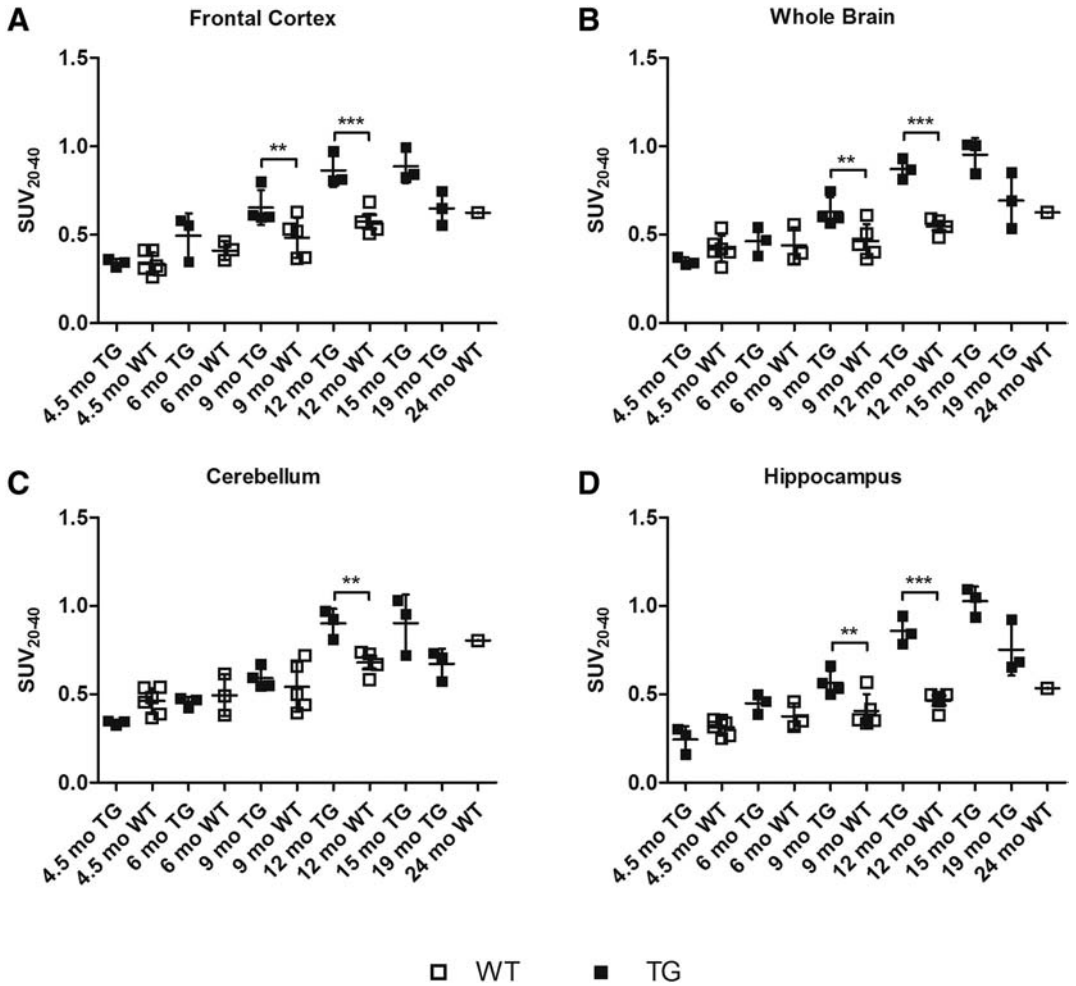

Fig. 3. SUVs of TG and WT animals at different ages (n = 1–6), averaged over 20–40 min in the; A) Frontal cortex, B) Whole brain, C) Cerebellum and D) Hippocampus. * are used to denote the level of significance between WT and TG. *p < 0.05,**p < 0.01, ***p < 0.001.

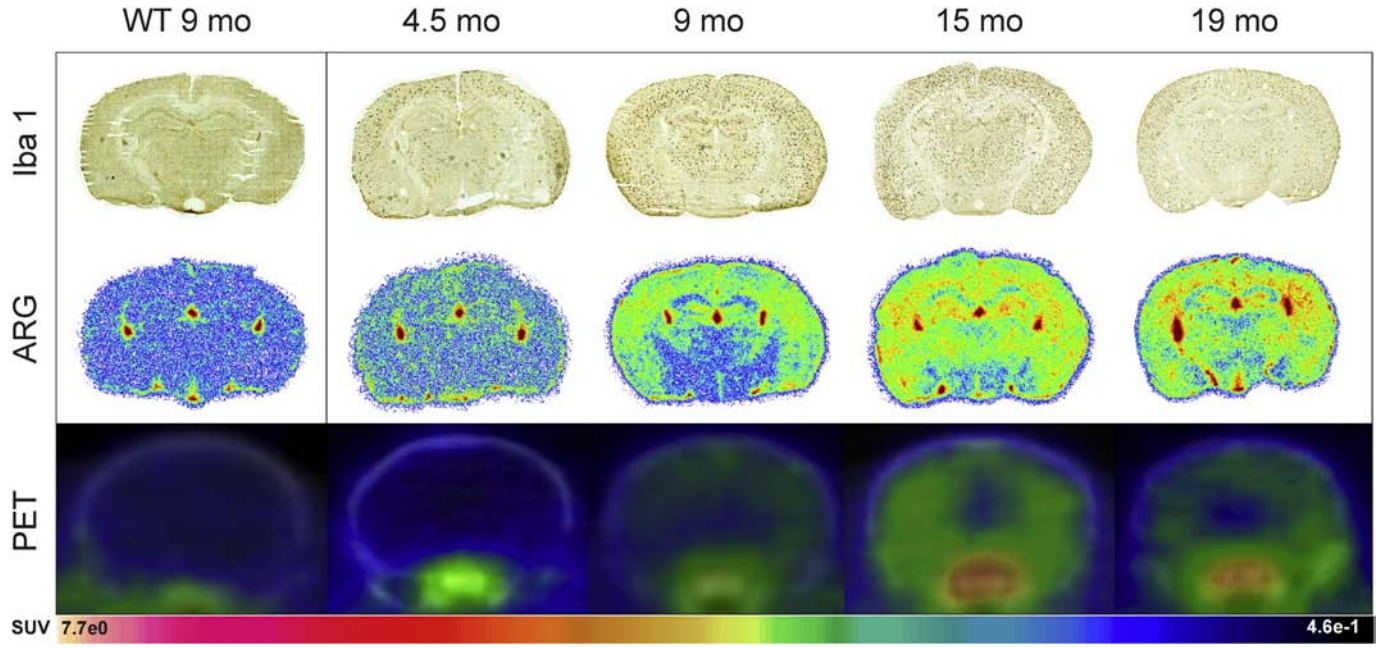

Fig. 4. Immunohistochemical stainings (Iba 1) and autoradiography images (ARG) of the same coronal sections for 9 mo WT and 4.5, 9, 15 and 19 mo TG mouse brains on the level of hippocampus, thalamus and hypothalamus. The 9 mo WT and 4.5, 9, 15 and 19 mo TG animals were administered with 6.9 ± 1.0 MBq of [^{18}F]F-DPA respectively, while under isoflurane anaesthesia. The coronal PET/CT images at the level of the HIPP are summed over 20–40 min after injection.

LV/HYP ratio of pre-treated mice was also significantly lower ($p = 0.029$) compared to non-pre-treated animals.

3.4. Biodistribution

The highest uptake in peripheral tissues was observed in the adrenals, lungs and kidneys. Moderate uptake was evident in bone (skull). The high uptake in the liver, gallbladder and intestine indicated that the radioactivity was excreted *via* the hepatobiliary tract (Fig. 8).

3.5. Radiometabolite TLC analysis

Two polar radiometabolites were clearly visible in the plasma with R_f values of 0.60 and 0.65. These accounted for, on average, a total of 25% of the remaining activity, 60 min after injection of the tracer, while the unchanged tracer (R_f value: 0.80) accounted for >70% (Fig. 9A). In the brain, no radiometabolites were observed at any time point (Fig. 9B).

4. Discussion

The APP/PS1-21 AD mice display plaque formation in the CTX at 6 wk, in HIPP at 2–3 mo and in the brain stem at 4–5 mo of age, with the number of neocortical microglia increasing threefold from 1 to 8 mo of age [16]. The previously reported lack of any difference between the amyloid burden of male and female animals [16] did not discourage the use of a mixture of males and females. Since it was seen in a previous study that the uptake of [^{18}F]DPA-714 in this model of disease only increases until 12 mo [14] and in the interest of ethical reduction of experimental animals, late WT ages were not studied.

The TACs, SUVs and ROI/HYP autoradiography ratios vary with age in TG animals (Figs. 2, 3 and 5), these together with the correlations carried out between tracer uptake and age (Supplementary Fig. 1) provide an idea of how neuroinflammation progresses with plaque formation in this particular model of disease.

In contrast to previously reported data obtained with [^{18}F]DPA-714 [14], it was found that uptake of the tracer in the CB varies with age. Although this variation does not present a statistically significant increase between adjacent age-groups, linear regression analysis (Supplementary Fig. 1) demonstrates that there is a significant increase over a 20 mo perspective. Hence, if the cerebellum would be used as a reference region, it would skew the resulting data. Due to the faster washout of [^{18}F]F-DPA compared to [^{18}F]DPA-714 [11], [^{18}F]F-DPA can better differentiate specific uptake in the CB and how it varies with age. Immunohistochemical staining for Iba1 (Fig. 4) demonstrated that the HYP is clear of pathology and hence can provide suitable reference region.

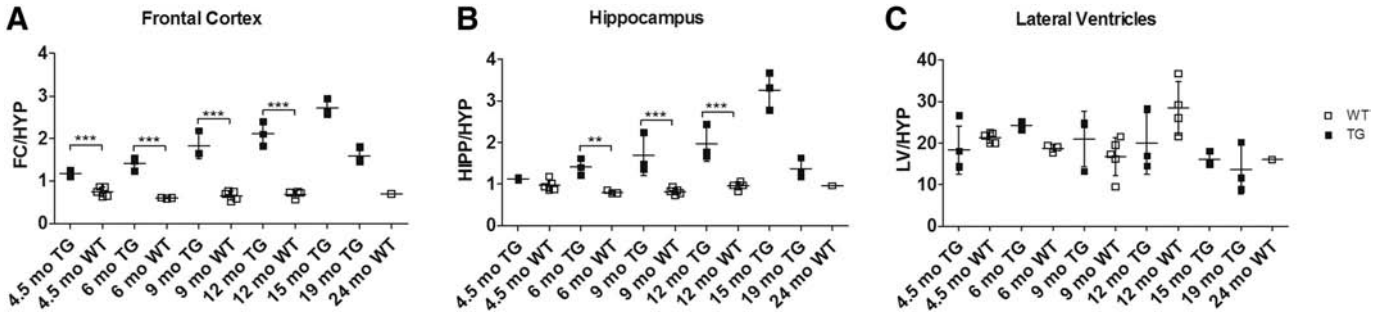

Fig. 5. *Ex vivo* brain autoradiography ratios of TG and WT animals at different ages (n = 1–5). The ROI to hypothalamus (HYP) ratios presented are for the A) Frontal cortex (FC), B) Hippocampus (HIPP) and C) Lateral ventricles (LV). ***p < 0.001.

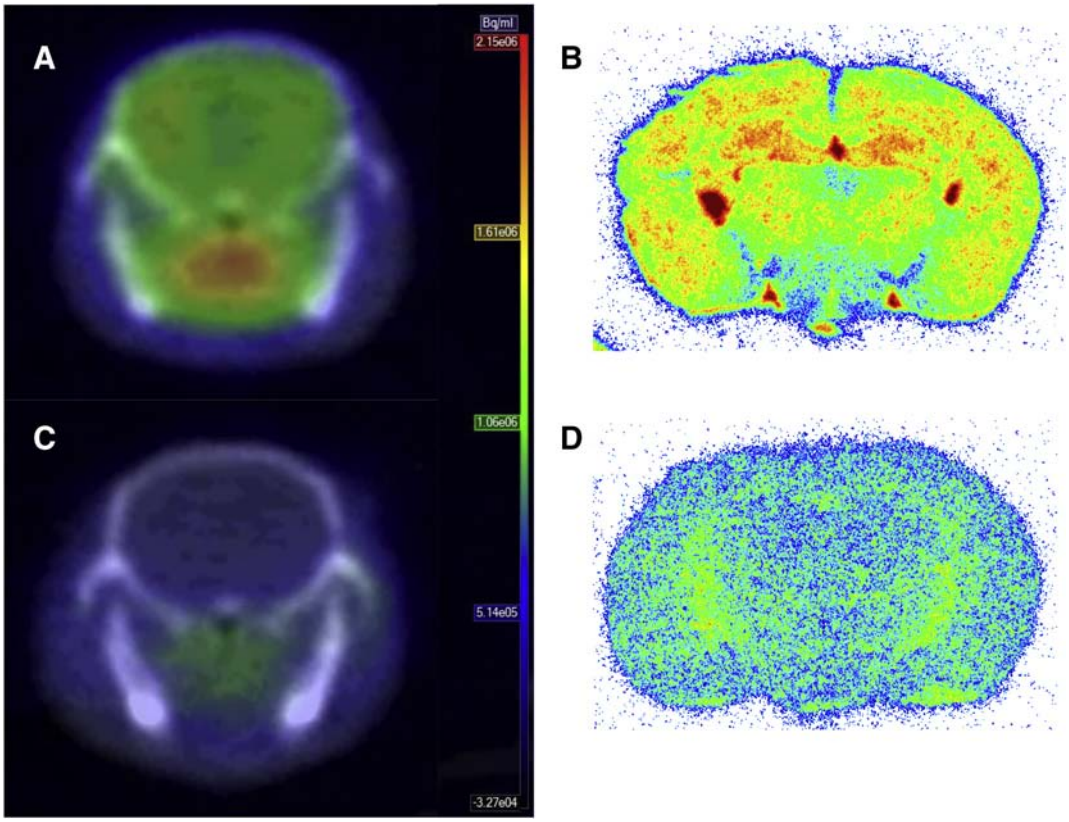

Fig. 6. *In vivo* (A and C) and *ex vivo* brain autoradiography (B and D) scans of 15 mo TG (A and B) and 15 mo TG pre-treated with PK11195 (C and D). The animals in images A and C were administered with 7.2 and 7.5 MBq of [^{18}F]F-DPA respectively, while under isoflurane anaesthesia. The PET images are summed over 20–40 min after injection.

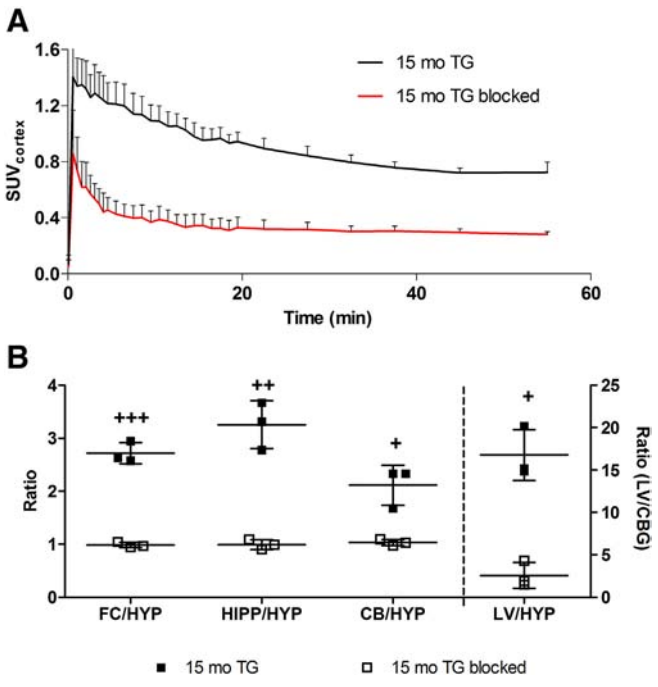

Fig. 7. Results of the blocking study; A) Cortical TACs of 15 mo TG (n = 3; solid) and 15 mo TG pre-treated with PK11195 (n = 3; dashed) and B) *Ex vivo* brain autoradiography region of interest (ROI)/Hypothalamus ratios for the Frontal cortex (FC), Hippocampus (HIPP), Cerebellum (CB) and Lateral ventricles (LV) showing decreased uptake in the brains of animals pretreated with PK11195. LV/HYP ratios are plotted on the right y-axis due to the markedly higher uptake in the LV resulting from high numbers of mitochondria in choroid plexus epithelials. 15 mo TG (solid) and 15 mo TG blocked (open). +p < 0.05, ++p < 0.01, +++p < 0.001.

Due to the proximity of the HYP to the pituitary gland, the high uptake of radioactivity in the pituitary gland (Figs. 4 and 6A) and resulting spill-over of signal, the HYP cannot be used as a reference region to calculate ratios for *in vivo* data. The higher resolution of autoradiography allows the reference region to be selected with greater precision and avoids the high signal spill-over from the pituitary (Fig. 4).

The first significant difference between the *in vivo* $SUVs_{20–40}$ of age-matched TG and WT animals is seen only at 9 mo and it is not possible to determine any significant difference for earlier age groups (Fig. 3), this may be due to the relatively low n. However the ROI/HYP ratios (Fig. 5) calculated from the *ex vivo* autoradiographs demonstrate that there is already a significant difference in the uptake of [^{18}F]F-DPA in the FC in age-matched healthy and diseased animals as young as 4.5 mo. The latter finding is in accordance with the description of this particular model in previous literature [16]. This difference between imaging methodologies arises from the higher sensitivity and spatial resolution of autoradiography compared to PET. However despite this difference the results showed a good positive correlation between *in vivo* PET and *ex vivo* autoradiography data for TG animals.

The APP/PS1-21 model has previously been studied using [^{18}F]DPA-714 and [^{18}F]FDG [14]. In this previous study the results obtained with [^{18}F]DPA-714 were presented as VOI/CB ratios, and showed significant differences in the cortex already at 6 mo, but significant differences HIPP only became apparent at later ages.

The consistently high uptake of [^{18}F]F-DPA in the LV (Fig. 5C) is due to the many functions of the choroid plexus (CP). The CP is responsible for the production of cerebrospinal fluid (CSF) and hence, there is much active transport of compounds across the CP in and out of the CSF. This active transport naturally requires energy that is provided by the vast amounts of mitochondria present in the CP epithelial cells [26]. These same mitochondria are responsible for the high accumulation of [^{18}F]F-DPA.

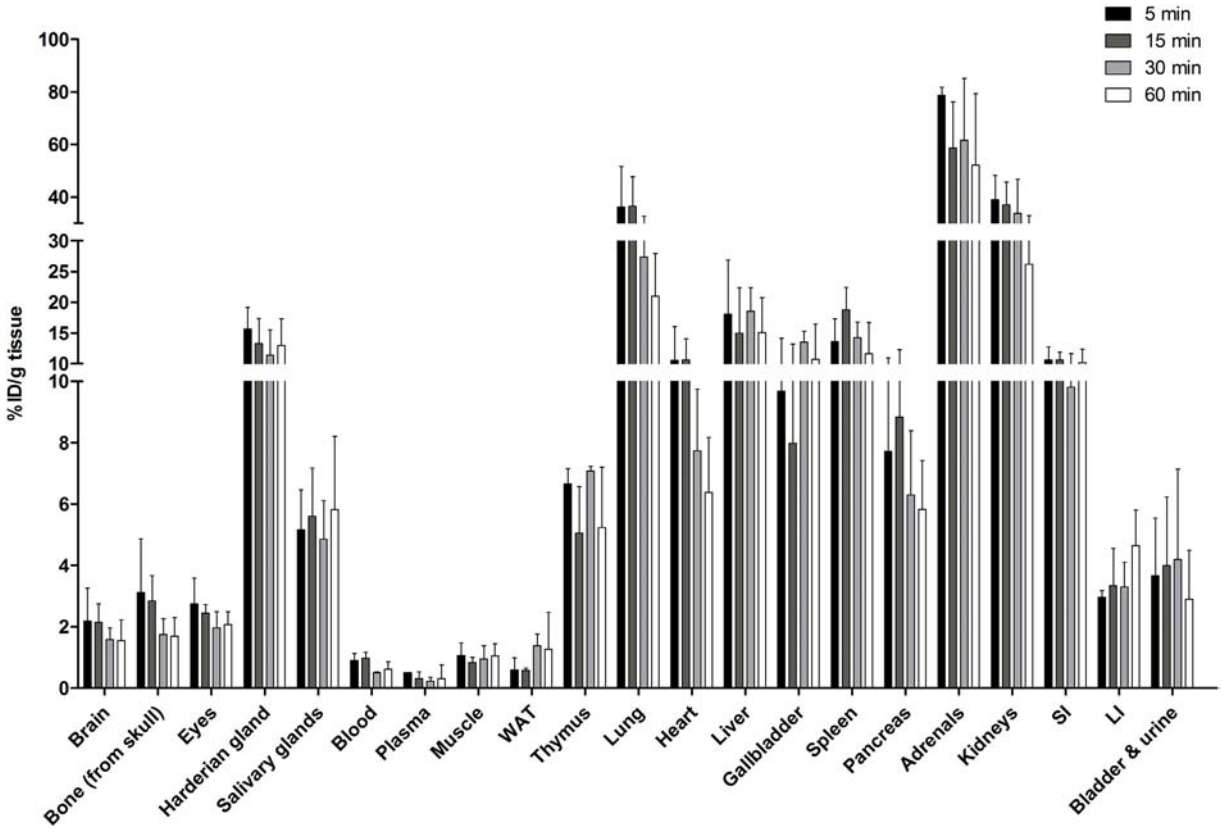

Fig. 8. *Ex vivo* biodistribution of radioactivity in TG mice presented as %ID/g tissue at 5 (n = 3), 15 (n = 3), 30 (n = 3) and 60 (n = 19) min after tracer injection. WAT = white adipose tissue, SI = small intestine, LI = large intestine.

Despite their differences, both of the imaging methodologies show that the trend of increasing [^{18}F]F-DPA uptake in TG animals only continues until 12–15 mo. In every case, there is a decrease between the 15 and 19 mo TG age points, which may result from an age-related decrease in the activation of microglia, changes in brain perfusion, the build-up of amyloid plaques to such an extent that there is decrease in the proportion of tissue that can undergo neuroinflammation or a combination of these factors. This reflects the previous findings [14,24] that TSPO expression does not continue to increase in very old animals despite a continuing increase in amyloidosis.

Previously, the ability of PK11195 to block [^{18}F]F-DPA was studied in a rat model of ischemic stroke with high levels of inflammation [12], the data presented herein further expands on this by studying the blocking effect in a transgenic model of disease with a chronic low level of inflammation, the APP/PS1-21 mice. Pretreatment with PK11195 results in saturation of the TSPO receptors, blocking them for [^{18}F]F-DPA occupancy. The *in vivo* PET and *ex vivo* autoradiography images (Fig. 6) reveal that there is an absence of specific binding in the brains of 15 mo TG mice that were pre-treated with PK11195 (Fig. 6 C and D) when compared to the non-pretreated 15 mo TG mice (Fig. 6 A and B).

The derived cortical TACs (Fig. 7A) further show that both the initial peak as well as subsequent binding of [^{18}F]F-DPA in the brains of the animals pre-treated with PK11195 are lower than for the 15 mo TG group. The autoradiography ROI/HYP ratios (Fig. 7B) confirm that the blocking results in a significantly decreased tracer-uptake in all the brain regions studied. The ROI/HYP uptake ratios of around 1 for the different brain regions prove that the blocking is successful and that there is a homogeneous distribution of the [^{18}F]F-DPA in the brain. In the case of the LVs, while most of the specific uptake has been blocked by the PK11195, due to the vast amounts of TSPO present in the ventricles the blocking here is not complete and the LV/HYP uptake ratios for the pre-treated animals are still >1.

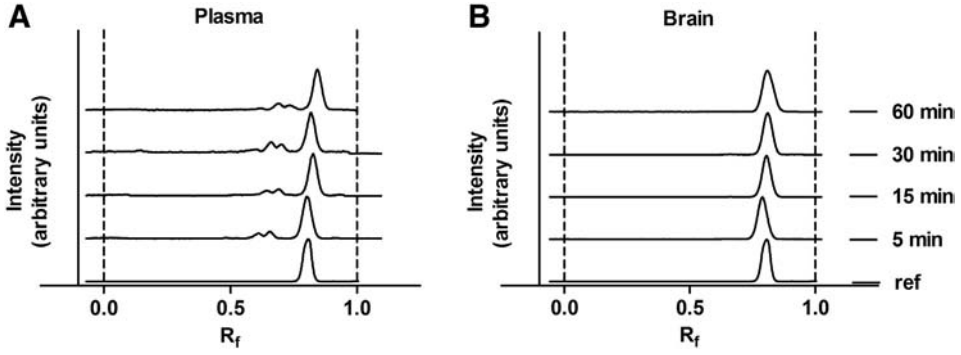

Fig. 9. RadioTLC chromatograms of A) Plasma and B) Brain homogenate carried out at 5, 15, 30 and 60 min after tracer administration. Two radiometabolites which are more polar than the unchanged tracer, R_f values: 0.60 and 0.65, can be seen in the plasma, but no radiometabolites could be observed in the brain at any time point. Chromatogram of unmetabolised ^{18}F-F-DPA (R_f = 0.80) included for reference.

In the *ex vivo* biodistribution (Fig. 8), the highest uptake of radioactivity can be seen in TSPO-rich organs such as the adrenals, lungs and kidneys. This, together with the lack of any accumulation of radioactivity in the bone, is in line with previously reported findings [12]. The accumulation of radioactivity with time in the intestine shows that the tracer and ^{18}F-containing metabolites are excreted mainly through the hepatobiliary tract. The lack of accumulation of activity in the bone suggests that metabolism of the tracer does not occur by defluorination, *i.e.* cleavage of the radioactive label, forming the fluoride that would be taken up in the bone and cause an accumulation of radioactivity.

The TLC analysis of radiometabolites in plasma and brain homogenates is the first instance of such a study being performed in mice. The results of these TLC radiometabolite analyses of plasma are in agreement with previously reported [^{18}F]F-DPA-radiometabolite data from rats [11] . Two radiometabolites which are more polar than the unchanged tracer are clearly visible. Identification of these metabolites was not performed. In contrast to previously reported results in rats, neither of these radiometabolites are observed in the brain at any time point. Previously, in rats, a small amount of radioactivity (6.2 ± 0.2%) can be attributed to compounds other than unchanged [^{18}F]F-DPA at 60 min after tracer injection. Since >99% of the radioactivity in the mouse brain can be attributed to the unchanged [^{18}F]F-DPA, we can conclude that in mice, the radiometabolites poorly cross the blood-brain barrier into the brain and that the metabolism of [^{18}F]F-DPA in the brain is slow enough to not interfere with the *in vivo* and *ex vivo* imaging.

The [^{18}F]F-DPA tracer, synthesised by the previously described electrophilic labelling procedure [11], was obtained with A_ms, yields and radiochemical purity in accordance with the previously reported data. The A_m of the [^{18}F]F-DPA obtained was only around 13-fold lower than that achieved by the previously reported nucleophilic method [12]. Due to the high abundance of the TSPO target, we believed that the relatively low A_m would not present any significant obstacles with regards to imaging using [^{18}F]F-DPA produced by the electrophilic route. This hypothesis was proven by the data presented herein, as a higher uptake of [^{18}F]F-DPA can be clearly seen in the brains of TG animals compared to their age-matched WT counterparts, at 4.5 mo by *ex vivo* autoradiography but later at 9 mo by *in vivo* imaging. Furthermore, this labelling position has only recently become accessible by a nucleophilic route [12,27] and hence work on the preclinical comparison of [^{18}F]F-DPA produced by electrophilic and nucleophilic methods has been initiated [27].

5. Conclusions

The study presented herein sheds further light on both the use of [^{18}F]F-DPA for the imaging of neuroinflammation as well as the APP/PS1-21 mouse model used, since the age-related change in neuroinflammation has not been previously studied in this model of AD using [^{18}F]F-DPA.

This study corroborates previously reported data, such as the biodistribution of [^{18}F]F-DPA, showing the highest accumulation in TSPO-rich organs in mice, and the blocking of specific [^{18}F]F-DPA uptake by pretreatment with PK11195 [12]. Furthermore, the electrophilic labelling methodology employed allows the facile and synthetically robust introduction of the fluorine-18 label directly on the aromatic ring, a position that has been shown to offer a relatively high degree of metabolic stability with respect to cleavage of the radioactive label [11]. This increased metabolic stability has also been further demonstrated in this study since no radio-metabolites were observed in the brain at any of the time points studied.

In this study it was shown that the A_m of the final [^{18}F]F-DPA product is sufficient for the successful and accurate imaging of neuroinflammation in this model of AD. Specifically, neuroinflammation and the pathology responsible for it can be detected by *ex vivo* autoradiography imaging already at 4.5 mo in this particular model of AD. The hypothalamus can be used as a reference region for *ex vivo* data. However due to the high accumulation of radioactivity in the pituitary gland which results in spill-over of signal, the hypothalamus cannot be used as a reference region for *in vivo* data. Furthermore, due to the lower sensitivity and worse spatial resolution of *in vivo* PET, compared to *ex vivo* autoradiography, the difference between WT and TG animals can only be detected in older ages *in vivo*.

Ethical approval

The study was approved by the Animal Experiment Board of the Province of Southern Finland (license numbers: ESAVI/3899/04.10.07/2013 and ESAVI/4660/04.10.07/2016) and animal care complied with the guidelines of the International Council of Laboratory Animal Science (ICLAS).

Availability of data and material

Please contact author for data requests.

Funding

This study was financially supported by a project fund from the European Commission Seventh Framework Programme FP7-PEOPLE-2012-ITN-RADIOMI-316882 and HEALTH-F2-2011-278850 (INMiND), by a clinical grant from the Turku University Hospital Education and Research Foundation (EVO, grant no 13250), and by the Academy of Finland (grant nos. 266891 and 310962).

Appendix A. Supplementary data

Supplementary data to this article can be found online at https://doi.org/10.1016/j.nucmedbio.2018.09.001.

References

[1] Papadopoulos V, Baraldi M, Guilarte TR, Knudsen TB, Lacapère JJ, Lindemann P, et al. Translocator protein (18 kDa): new nomenclature for the peripheral-type benzodiazepine receptor based on its structure and molecular function. Trends Pharmacol Sci 2006;27:402–9.
[2] Anholt R, Pedersen P, De Souza E, Snyder S. The peripheral-type benzodiazepine receptor. Localization to the mitochondrial outer membrane. J Biol Chem 1986;261:576–83.
[3] Banati RB. Visualizing microglial activation in vivo. Glia 2002;40:206–17.
[4] Giatzakis C, Papadopoulos V. Differential utilization of the promoter of peripheral-type benzodiazepine receptor by steroidogenic versus nonsteroidogenic cell lines and the role of Sp1 and Sp3 in the regulation of basal activity. Endocrinology 2004;145:1113–23.
[5] Doorduin J, Klein HC, Dierckx RA, James M, Kassiou M, de Vries EFJ. [^{11}C]-DPA-713 and [^{18}F]-DPA-714 as new PET tracers for TSPO: a comparison with [^{11}C]-(*R*)-PK11195 in a rat model of herpes encephalitis. Mol Imaging Biol 2009;11:386–98.
[6] Doorduin J, Klein HC, de Jong JR, Dierckx RA, de Vries EFJ. Evaluation of [^{11}C]-DAA1106 for imaging and quantification of neuroinflammation in a rat model of herpes encephalitis. Nucl Med Biol 2010;37:9–15.
[7] Buck JR, McKinley ET, Hight MR, Fu A, Tang D, Smith RA, et al. Quantitative, preclinical PET of translocator protein expression in glioma using ^{18}F-*N*-fluoroacetyl-*N*-(2,5-dimethoxybenzyl)-2-phenoxyaniline. J Nucl Med 2011;52:107–14.
[8] Pottier G, Bernards N, Dollé F, Boisgard R. [^{18}F]DPA-714 as a biomarker for positron emission tomography imaging of rheumatoid arthritis in an animal model. Arthritis Res Ther 2014;16:R69.
[9] Alam MM, Lee J, Lee S-Y. Recent progress in the development of TSPO PET ligands for neuroinflammation imaging in neurological diseases. Nucl Med Mol Imaging 2017;51:283–96.
[10] Lagarde J, Sarazin M, Bottlaender M. In vivo PET imaging of neuroinflammation in Alzheimer's disease, 125; 2018; 847–67.
[11] Keller T, Krzyczmonik A, Forsback S, Picón FR, Kirjavainen AK, Takkinen J, et al. Radiosynthesis and preclinical evaluation of [^{18}F]F-DPA, a novel pyrazolo[1,5a]pyrimidine acetamide TSPO radioligand, in healthy Sprague Dawley rats. Mol Imaging Biol 2017;19:736–45.
[12] Wang L, Cheng R, Fujinaga M, Yang J, Zhang Y, Hatori A, et al. A facile radiolabeling of [^{18}F]FDPA via spirocyclic iodonium ylides: preliminary PET imaging studies in preclinical models of neuroinflammation. J Med Chem 2017;60:5222–7.
[13] James ML, Fulton RR, Vercoullie J, Henderson DJ, Garreau L, Chalon S, et al. DPA-714, a new translocator protein-specific ligand: synthesis, radiofluorination, and pharmacologic characterisation. J Nucl Med 2008;49:814–22.
[14] Takkinen JS, López-Picón FR, Al Majidi R, Eskola O, Krzyczmonik A, Keller T, et al. Brain energy metabolism and neuroinflammation in ageing APP/PS1-21 mice using longitudinal ^{18}F-FDG and ^{18}F-DPA-714 PET imaging. J Cereb Blood Flow Metab 2017;37:2870–82.

[15] Deleye S, Waldron AM, Verhaeghe J, Bottelbergs A, Wyffels L, Van Broeck B, et al. Evaluation of small-animal PET outcome measures to detect disease modification induced by BACE inhibition in a transgenic mouse model of Alzheimer disease. J Nucl Med 2017;58:1977–83.
[16] Radde R, Bolmont T, Kaeser SA, Coomaraswamy J, Lindau D, Stoltze L, et al. Aβ42-driven cerebral amyloidosis in transgenic mice reveals early and robust pathology. EMBO Rep 2006;7:940–6.
[17] Rupp NJ, Wegenast-Braun BM, Radde R, Calhoun ME, Jucker M. Early onset amyloid lesions lead to severe neuritic abnormalities and local, but not global neuron loss in APPPS1 transgenic mice. Neurobiol Aging 2011;32:2324.e1-6.
[18] Peyronneau MA, Saba W, Goutal S, Damont A, Dollé F, Kassiou M, et al. Metabolism and quantification of [^{18}F]DPA-714, a new TSPO positron emission tomography radioligand. Drug Metab Dispos 2013;41:122–31.
[19] Medran-Navarrete V, Bernards N, Kuhnast B, Damont A, Pottier G, Peyronneau MA, et al. [^{18}F]DPA-C5yne, a novel fluorine-18-labelled analogue of DPA-714: radiosynthesis and preliminary evaluation as a radiotracer for imaging neuroinflammation with PET. J Labelled Compd Radiopharm 2014;57:410–8.
[20] Tang D, McKinley ET, Hight MR, Uddin MI, Harp JM, Fu A, et al. Synthesis and structure-activity relationships of 5,6,7-substituted pyrazolopyrimidines: discovery of a novel TSPO PET ligand for cancer imaging. J Med Chem 2013;56:3429–33.
[21] Tang D, Li J, Buck JR, Tantawy MN, Xia Y, Harp JM, et al. Evaluation of TSPO PET ligands [^{18}F]VUIIS1009A and [^{18}F]VUIIS1009B: tracers for cancer imaging. Mol Imaging Biol 2017;19:578–88.
[22] Tang D, Fujinaga M, Hatori A, Zhang Y, Yamasaki T, Xie L, et al. Evaluation of the novel TSPO radiotracer 2-(7-butyl-2-(4-(2-[^{18}F]fluoroethoxy)phenyl)-5-methylpyrazolo[1,5-a]pyrimidin-3-yl)-*N*,*N*-diethylacetamide in a preclinical model of neuroinflammation. Eur J Med Chem 2018;150:1–8.
[23] Mouse MRI brain template. MRM NAt Mouse Brain Database. McKnight Brain Institutehttp://brainatlas.mbi.ufl.edu/Database/; 2005, Accessed date: 17 May 2013.
[24] López-Picón FR, Snellman A, Eskola O, Helin S, Solin O, Haaparanta-Solin M, et al. Neuroinflammation appears early and then plateaus in a mouse model of Alzheimer's disease shown by PET imaging. J Nucl Med 2018;59:509–15.
[25] Hardwick MJ, Chen M, Baidoo K, Pomper MG, Guilarte TR. In vivo imaging of peripheral benzodiazepine receptors in mouse lungs: a biomarker of inflammation. Mol Imaging 2005;4:432–8.
[26] Cornford EM, Varesi JB, Hyman S, Damian RT, Raleigh MJ. Mitochondrial content of choroid plexus epithelium. Exp Brain Res 1997;116:399–405.
[27] Keller T, López-Picón FR, Krzyczmonik A, Forsback S, Kirjavainen AK, Takkinen J, et al. Nucleophilic and electrophilic syntheses of [^{18}F]F-DPA. J Labelled Compd Radiopharm 2017;60(Suppl. 1):S382.